Indian dust-rain storm: Possible influences of dust ice nuclei on deep convective clouds

Tiangang Yuan [a], Jianping Huang [a,b,*], Jiahui Cao [a], Guolong Zhang [a], Xiaojun Ma [c]

[a] Key Laboratory for Semi-Arid Climate Change of the Ministry of Education, College of Atmospheric Sciences, Lanzhou University, Lanzhou 730000, China
[b] Collaborative Innovation Center for Western Ecological Safety, Lanzhou University, Lanzhou 730000, China
[c] Innovation Center of Ocean-Atmosphere System Observation and Prediction, Zhuhai Fudan Innovation Institute, Zhuhai 519000, China

HIGHLIGHTS

- A dust-rain storm erupted over Northwest India and caused heavy rainfall.
- Dust layer and ice cloud coexisted at 11 km over the foothill of Tibetan Plateau.
- Dust ice nuclei may invigorate the deep clouds by glaciating the supercooled cloud.

GRAPHICAL ABSTRACT
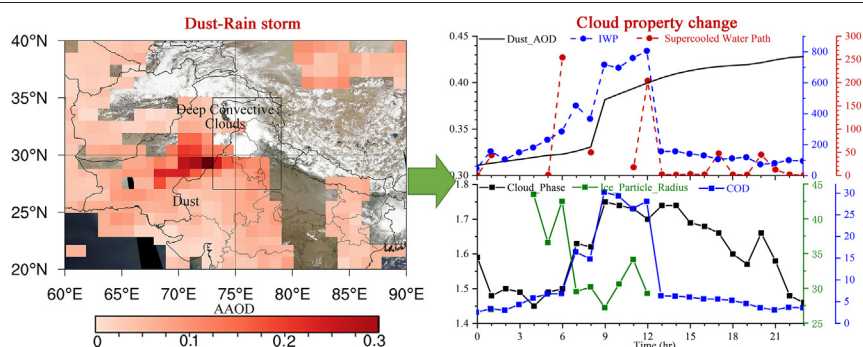
ARTICLE INFO

ABSTRACT

Estimating the influence of dust aerosol on clouds, especially deep convective clouds which is closely related to heavy precipitation, still has large uncertainties due to the lack of adequate direct measurements. In this study, a typical dust storm along with thunderstorm (referred to dust-rain storm), occurred in Northwest India on May 2, 2018, was selected to explore the possible effects of dust aerosol on deep convective cloud by combining a series of satellite retrievals and reanalysis data. Results showed that dust aerosol and moisture were carried to Northwest India by southwesterly wind at 700 hPa and easterly wind along south foothill of Himalayas at 850 hPa, respectively, and then were lifted to upper level of the cloud by robust updraft induced by the deep convection and secondary circulation driven by the upper-level westerly jet. The injection of dust is likely to transfer supercooled water cloud into ice cloud as effective ice nuclei, hence increasing the cloud ice water path and cloud optical depth but decreasing ice particle radius in the cloud. The latent heat released by this phase-change process would enhance the deep convection and further cause heavy rainfall in northern India by drawing moisture from surrounding region. Although we cannot eliminate the effect of large-scale dynamics, this study highlighted the role of dust aerosol in invigorating the deep convective clouds as ice nuclei, providing observation evidence for the investigation of aerosol-cloud-precipitation interaction.

© 2021 Elsevier B.V. All rights reserved.

1. Introduction

On May 2, 2018, a typical dust storm along with strong winds and thunderstorm (hereafter referred to dust-rain storm) hit parts of Rajasthan, Uttar Pradesh, and adjoining regions in northern India, killing over 120 people and injuring hundreds more in some states. This disaster

* Corresponding author at: Key Laboratory for Semi-Arid Climate Change of the Ministry of Education, College of Atmospheric Sciences, Lanzhou University, Lanzhou 730000, China.

E-mail address: hjp@lzu.edu.cn (J. Huang).

again reminds us of the catastrophic damage caused by extreme weather to human life under the context of global warming. It is reported that the frequency of annual extreme weather events including floods and heat waves, and extreme rain events presented a rising trend over the past few decades in India (Ray et al., 2019; Goswami et al., 2006), which favors the increase in total precipitation during Indian Summer Monsoon (Pattanaik and Rajeevan, 2010). The floods made up the highest mortality of 46.1% among all extreme weather events and resulted in significant economic loss (Ray et al., 2021; Roxy et al., 2017).

Since 1960s, the drylands have expanded in semiarid regions and it will account for 50% of the global land at the end of this century (Huang et al., 2016a, 2016b). The warming rate over global drylands is 20–40%, larger than that over humid regions, indicating the drylands will suffer stronger warming risks such as desertification (Huang et al., 2017a, 2017b). Consequently, the dust aerosol emitted from these areas would increase, and then modulate Earth's radiative budget, which in turn influences regional climate (Chen et al., 2017; Kok et al., 2017). Due to its atmospheric heating and surface cooling, daytime planetary boundary layer stability tended to be increased by 90 m in North China (Liu et al., 2016). The weakness of wind speed induced by dust aerosol exacerbates the winter haze over eastern China (Yang et al., 2017). Dust radiative forcing also reduces surface air temperature over Indian peninsula and Northwest China where there is an increasing vapor belt accompanying by intensified precipitation (Wu et al., 2010). Different from the decrease in wind speed at 10 m, surface temperature and dust cycle in East Asia, dust-radiation interaction in North Africa presented opposite effects, which is related to surface property, aerosol vertical distribution and size distribution (Xie et al., 2018). Latest research observed a significant role of dust aerosol in inhibiting tropical cyclone genesis over North Atlantic Ocean Basin through reducing sea surface temperature and low-level humidity, increasing midlevel moisture, inducing positive relative vorticity and wind shear (Sun and Zhao, 2020).

The North/Northwest India witnessed the highest frequency of dust storms during pre-monsoon compared to other time periods (Sikka, 1997). Considerable observations have shown that dust aerosols in this region is mainly originated from nearby Thar desert or remote Arabian Peninsula by long distance transport along with westerly/southwesterly wind (Sijikumar et al., 2016; Gautam et al., 2009; Kedia et al., 2018), among of which, the Thar desert is responsible for the frequent heavy dust storms in Indo-Gangetic Plain (IGP) (Washington et al., 2003; Dey et al., 2004). Dust transported to IGP can intermingle with the local carbonaceous aerosols, leading to stronger absorption, especially in urban areas (Gautam et al., 2011; Kedia et al., 2014). Kumar et al. (2014) estimated that the direct radiative forcing induced by dust over India was 5.1 ± 3.3 W m^{-2} in the atmosphere, twice more than five-year average value over Taklimakan desert (~ 2.5 W m^{-2}) (Chen et al., 2017). Over northwestern parts including India and Pakistan, atmospheric heating induced by dust aerosol from Arabian Peninsula was also obvious (Kedia et al., 2018). The atmospheric heating of dust aerosol over northern India can advance the India rainy season (Lau et al., 2006). They also enhance the deep convection and cloud cover by increasing moisture convergence when below a cloud layer, but weaken the cumulus clouds when above a cloud layer (referred to "Semidirect Effect") (Huang et al., 2014).

It is well known that dust aerosol is effective Ice Nuclei (IN) (DeMott et al., 2003), as well as Cloud Condensation Nuclei (CCN) when coated with soluble pollutants such as sulfate and nitrate (Tobo et al., 2010; Liu et al., 2011). Aerosols restrain precipitation as CNN in shallow clouds with smaller cloud droplets and less efficient coalescence (Guo et al., 2014; Li et al., 2016; Yang et al., 2019), but enhance precipitation when it comes to deep convective clouds (DCCs) by aerosol-induced invigoration effect (Rosenfeld et al., 2008; Heiblum et al., 2012; Peng et al., 2016). Recently, Fan et al. (2018) revealed that the invigoration theory is applicable for shallow water clouds under ultra-fine mode aerosol

pollution. However, knowledge about heterogeneous dust IN in DCC formation is still limited due to the lack of adequate measurements. Yin and Chen (2007) found that dust acting as IN can accelerate the ice-forming process and might further promote the development of precipitation when dust layer appears above −5 °C level using a cloud model. Based on 4-year Cloud-Aerosol Lidar and Infrared Pathfinder Satellite Observation (CALIPSO) and CloudSat combined dataset, Zhang et al. (2015) suggested that the dust glaciated mixed-phase clouds by supplying large amount of effective IN over East Asia. Y. Liu et al. (2019) revealed that aerosols dominated the decrease of daytime ice cloud droplet radius over the Tibetan Plateau from 2000 to 2015 using Clouds and the Earth's Radiant Energy System (CERES) data.

Although increasing effort has been paid to the impact of dust on cirrus cloud properties through long-term statistics or model simulation, the interaction between dust aerosol and DCCs which usually cause heavy rainfall, still has large uncertainty. In this study, the dust-rain storm provides us with an opportunity to gain an insight into this scientific question. We proposed a possible mechanism to explain the interaction between dust aerosol and DCC from the heterogeneous IN perspective by combining multiple satellite and reanalysis data. This paper is organized as follows: data and methodology are listed in Section 2; results are shown in Section 3; conclusions and discussion are illustrated in Section 4.

2. Data and methodology

2.1. Reanalysis data

The Modern-Era Retrospective Analysis for Research and Applications version 2 (MERRA-2) is the latest NASA atmospheric reanalysis dataset for satellite era and developed by Global Modeling and Assimilation Office (Gelaro et al., 2017). It has some improvements which are unavailable to previous MERRA dataset, such as aerosol assimilation for the entire period with the Goddard Earth Observing System Model, Version 5 (GEOS-5), version 5.12.4. Aerosol assimilation in MERRA-2 does improve the surface dust concentration and Aerosol Optical Depth (AOD). The vertical distribution of aerosols observed by CALIPSO and aircraft is also captured, which mean the high reliability of MERRA-2 aerosol data (Buchard et al., 2017). Recently, the accuracy of MERRA-2 dust data in exhibiting spatial-temporal evolution of dust events was also evaluated by comparing multiple satellite and ground-based observations including Moderate resolution Imaging Spectroradiometer (MODIS) (Sun et al., 2019) and Multi-Sensor Absorbing Aerosol Index data (L. Liu et al., 2019), Aerosol Robotic Network and National Urban Air Quality Real-time Publishing Platform and Hamawari-8 (W. Yao et al., 2020). The model utilizes a cubed-sphere horizontal discretization at a resolution of $0.5° \times 0.625°$ and the atmosphere is divided into 72 levels up to 0.01 hPa. Here, the hourly dust AOD, and 3-hourly dust concentration and wind field derived from MERRA-2 were used to explore the spatial-temporal distribution of dust aerosol.

The ERA5 is a new reanalysis data released by European Centre for Medium-range Weather Forecasting (ECMWF) in 2017 with considerable improvements over ERA-interim (Albergel et al., 2018). For instance, it provides higher spatial and temporal resolution (0.25° and 1-hourly, respectively) compared with ERA-interim (0.75° and 6-hourly). Besides, the major advancements are the 4D-Var data assimilation scheme, integrated forecasting IFS system, CY41r2 global spectrum model and more historical observation assimilated, all of which make the products more accurate (Huai et al., 2021). It has been extensively used in the investigation of aerosol properties over Australia (Yang et al., 2020), precipitation over China (Jiang et al., 2020) and the spatial-temporal variation of global clouds (B. Yao et al., 2020). In this study, we used hourly air temperature, wind speed, geopotential height, sea-level pressure, specific humidity and cloud ice water content on May 2, 2018 to analyze this event.

2.2. Satellite observations

As the successor of Tropical Rainfall Measuring Mission (TRMM), the Global Precipitation Measurement (GPM), launched in February 2014, starts to provide the next generation of precipitation products with some critical advancements. For example, it carries a dual-frequency precipitation radar with two high frequency bands (165.5 and 183.3 GHz) and a passive microwave imager, which allow it to detect light and solid precipitation over a large coverage (Huffman et al., 2019). The Integrated Multi-satellitE Retrievals for GPM (IMERG) "Final run" products incorporated the estimates of precipitation from other satellites and rain gauge corrections, and has the best quality-assured precipitation data. It also shows better performance in detecting extreme precipitation over TRMM (Fang et al., 2019). Thus, the latest version 06B GPM "Final run" products with the horizontal resolution of $0.1° \times 0.1°$ and half hour time interval on May 2, 2018 over South Asia, were used to demonstrate the evolution of convective precipitation.

The CALIPSO satellite was launched in April 2006 and carries the Cloud–Aerosol Lidar with Orthogonal Polarization (CALIOP) instrument which primarily retrieves vertical profile of aerosols and clouds by providing attenuated backscatter at 532 nm and 1064 nm (Cesana et al., 2016). It has the capability of distinguishing aerosol and cloud types. The CALIPSO level 2 aerosol and cloud profile products version 4.20 that passed the study region at 07:39 UTC and 20:03 UTC, May 2, 2018 are utilized to show the vertical structure of dust and clouds.

The CERES instrument is mainly designed to provide global observations for cloud and radiative flux by matching the cloud properties from MODIS onboard Aqua and Terra and geostationary (GEO) satellites (Wielicki et al., 1996). The Synoptic TOA and surface fluxes and clouds (SYN) products contain hourly gridded liquid and ice cloud properties such as cloud visible optical depth (COD), liquid water path (LWP), ice water path (IWP), ice particle radius (IPR), cloud phase and cloud top temperature at a resolution of $1° \times 1°$. There are several key improvements in CERES cloud algorithm in Ed4 version compared to that in Ed3A including high clouds and ice cloud (Chang et al., 2010; Yang et al., 2008).

The MODIS/Aqua corrected surface reflectance true color composite of Red Green and Blue (RGB) image in Fig. 1a is downloaded from NASA Global Imagery Browse Services. The Absorbing AOD (AAOD) at 500 nm embedded in MODIS true color image is used to represent the distribution of dust aerosol and is derived from ozone monitoring instrument (OMI) near-ultraviolet (UV) aerosol algorithm (OMAERUV) product retrieved by OMI onboard Aura satellite (Torres, 2008). The MODIS instrument onboard the Terra and Aqua satellites views the entire Earth surface every 1 to 2 days, acquiring the information of global aerosol and clouds (Platnick et al., 2003; Hsu et al., 2013). The level 2 dark target and deep blue combined AOD from MODIS onboard Aqua and Terra with a horizontal resolution of 10 km are selected to show the distribution of aerosols at 06:30 and 08:05 UTC, considering their better accuracy compared with ground observations. Correspondingly, the cirrus reflectance, cloud effective radius, cloud water path and cloud types obtained from MODQ21KM and MYDQ21KM products with a spatial resolution of 1 km and 5 min time interval are also used to illustrate the microphysical properties of the DCC.

2.3. In-situ measurements

The wind speed at 10 m, air temperature at 2 m, sea-level pressure with 3-h interval at Delhi weather station are obtained from the China Meteorological Administration (http://data.cma.cn/). We also used radio-sounding data from University of Wyoming (http://weather.uwyo.edu/upperair/sounding.html) at 00 UTC (local time, 5:30) and 12 UTC (local time, 17:30) in Delhi to describe the vertical profile of atmosphere stratification that supports the outbreak of dust storm and thunderstorm. The hourly surface $PM_{2.5}$ observations in Delhi are available from the United States Embassy (https://in.usembassy.gov/embassy-consulates/new-delhi/air-quality-data/).

2.4. Cloud phase identification

In this study, the CALIPSO level 2 vertical feature mask (VFM) data provides the vertical distribution of ice, water, and oriented ice crystal cloud along the CALIPSO orbit at two periods during this event. Hu et al. (2009) developed an algorithm for Supercooled Water Cloud (SWC) through utilizing CALIPSO cloud products. They found the relationship between SWC fraction and cloud midlayer temperature which is parameterized with Eq. (1).

$$p(T_{mid}) = 5.3608 + 0.4025T_{mid} + 0.08387T_{mid}^2 + 0.007182T_{mid}^3 \\ + 2.39 \times 10^{-4}T_{mid}^4 + 2.87 \times 10^{-6}T_{mid}^5 \qquad (1)$$

$$f(T) = \frac{1}{1 + e^{-p(T)}} \qquad (2)$$

where p(T) is polynomial fitting function between CALIPSO SWC fraction f(T) and cloud mid layer temperature. The SWC fraction can be estimated according to Eq. (2). Here, we followed Wang et al. (2019) who used the CALIPSO cloud layer mid-temperature to replace the original midlayer cloud temperature in Hu et al. (2009), and viewed the cloud with the SWC fraction more than 80% as SWCs. Notably, Wang et al. (2019) developed a newly time-continuous SWC algorithm using Himawari-8 geostationary satellite by introducing cloud effective radius and cloud Phase. Their results showed good performance in detecting SWC compared with Hu et al. (2009). However, coverage of Himawari-8 is limited and our study area are excluded, which makes us fail to try this method.

In CERES SYN1deg Ed4A product, the cloud particle phase can be applied to distinguish ice clouds from liquid cloud. In order to identify the SWC, we follow the method mentioned by Bodas-Salcedo et al. (2016) who elucidated that any liquid cloud whose cloud top temperature < 0 °C is recognized as SWC. Therefore, we viewed the cloud whose LWP > 0 and temperature < 0 as SWC and selected them from CERES and MODIS cloud products.

3. Results

3.1. Dust-rain Strom on May 2, 2018

On May 2, 2018, a severe dust storm and thunderstorm ripped across northern India: Rajasthan, Uttar Pradesh, Punjab, Delhi and Haryana (Fig. 1), resulting in the death of more than 120 lives and injuries to 300, collapse of the housing, uprooting trees and the damage of electric poles according to reports from India media (https://india.mongabay.com/2018/05/dust-storms-may-increase-in-india-due-to-climate-change/). The Indian Meteorological Department claimed that the instantaneous wind speed was over 100 km/h in Uttar Pradesh during this event, which is conductive to the emission and transport of dust aerosol to IGP. The visibility in Delhi dropped steeply from 2.7 km on May 1 to 1.6 km on May 2. It should be noted that IGP has experienced three dust storms during this month, among of which, this event is deadly over the past three decades in terms of the damage and intensity (Sarkar et al., 2019).

As indicated by MODIS composite images, the dust storm mainly originated from Thar desert where the AAOD soared to more than 0.3 and extended towards northern border of Pakistan and India. Meanwhile, a well-developed DCC (or thunderstorms), that was partially within thick dust layer and covered northwest India and eastern Pakistan including Punjab, Himachal Pradesh, Jammu and Kashmir where 12-hour (0–12 UTC) cumulative precipitation derived from GPM was 5–30 mm, was observed by MODIS image (Fig. 1a, b). It also caused heavy rainfall after 12 UTC in Delhi, Haryana and part of Rajasthan (Fig. S1). From the CALIPSO profile, we can see that the dust layer existed below 6 km over India at 07:39 UTC and it stretched to northeast margin of DCC (Fig. 1c). Notably, dust and ice cloud coexisted at the altitude of 11 km over foothill of Himalayan (29.88 °N, 79.6 °E) in
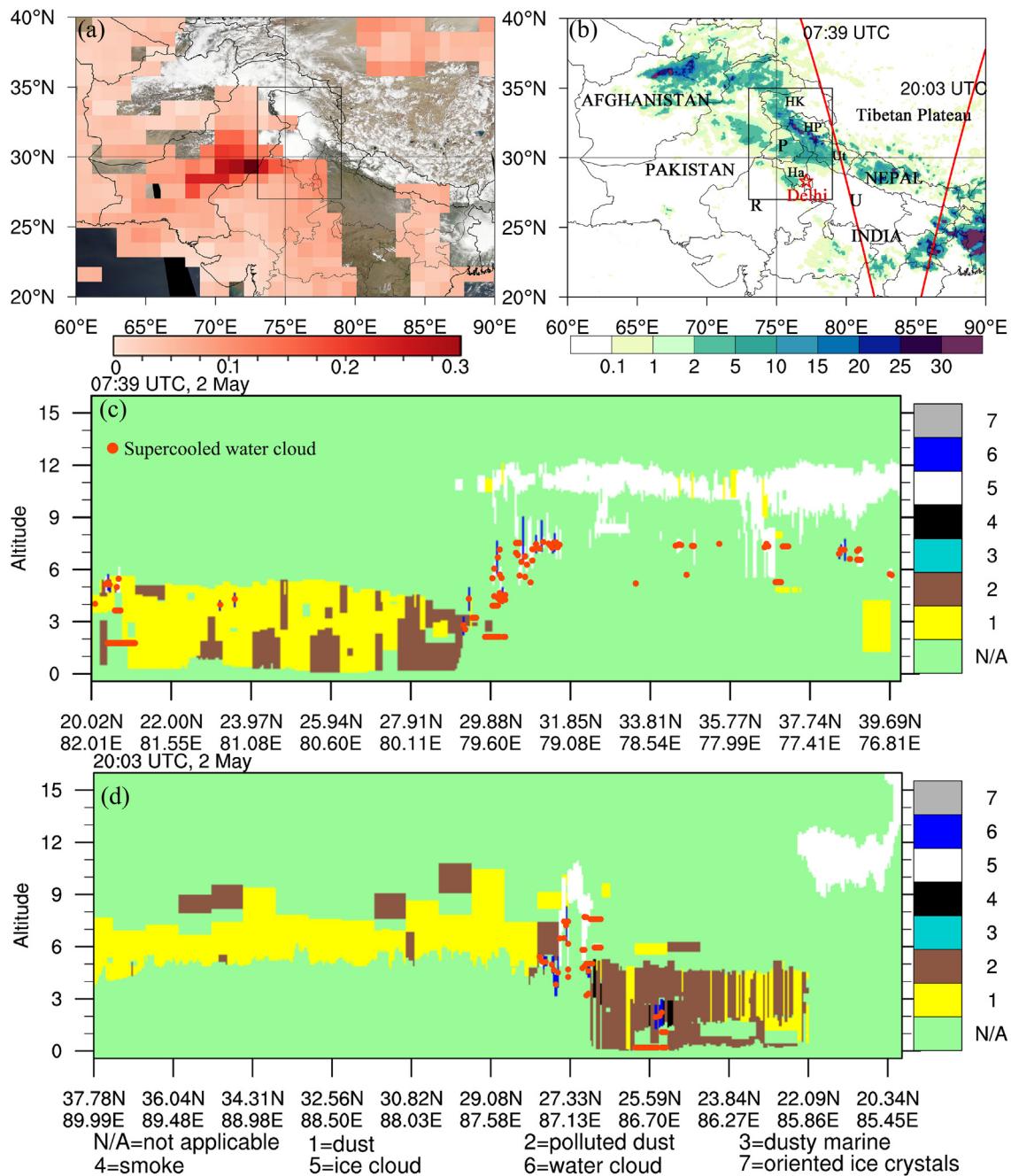
Fig. 1. Dust-rain storm observed by satellites. (a) MODIS RGB composite image overlaid by OMI AAOD at 500 nm, (b) GPM cumulative precipitation (mm) from 00 to 12 UTC, CALIPSO aerosol and cloud types at (c) 07:39 UTC and (d) 20:03 UTC, May 2, 2018. Orangered dots in (c) and (d) are supercooled water clouds selected from CALIPSO cloud products. Red star indicates the location of Delhi; red lines show the CALIPSO tracks; black box indicated the region this study focused on. The northern Pakistan, and several sates of Jammu and Kashmir (HK), Himachal Pradesh (HP), Punjab (P), Uttarakhand (Ut), Rajasthan (R), Uttar Pradesh (U), and Haryana (Ha) in India are influenced by this event. (For interpretation of the references to color in this figure legend, the reader is referred to the web version of this article.)

which the convective clouds developed. Near the south slope of the Himalayan, a large number of SWCs also intermingled with dust layer. The dust storm even moved to east India at night and most of dust mixed with anthropogenic aerosol, lifting to over 6 km (Fig. 1d). There are still some SWCs at this time. Along with mid-upper southerly wind, dust aerosol was even transported to the Tibetan Plateau across Himalayan between 2 and 3 May (Wang et al., 2020), which is why there is a dust layer appearing over the Tibetan Plateau depicted by the CALIPSO track at 20:03 UTC.

Fig. 2 demonstrates hourly evolution of meteorological conditions and PM$_{2.5}$ concentration in Delhi. The air temperature at 2 m saw an

increase to 37.6 °C at noontime (9 UTC, 14:30 Local Time), after which it experienced a remarkable decline to 20.2 °C at 15 UTC, indicating the cold air dominated this area during the period of 9 to 15 UTC. Nevertheless, the sea-level pressure dropped from 1008.1 hPa to 1001.8 hPa at 9 UTC (15: 30 Local Time), which means that the increasing incident solar radiation induced a low pressure. Exposure to the cold front, the wind speed over Delhi at 10 m rose to 9 m s^{-1}, a positive change of 5 m s^{-1}, along with an increase of 4.4 hPa at 15 UTC, respectively. The remarkable increase of wind speed and pressure brought more dust aerosol to Delhi, leading to a peak of PM$_{2.5}$ concentration (216 μg m^{-3}) at 13 UTC which is approximately five times more than
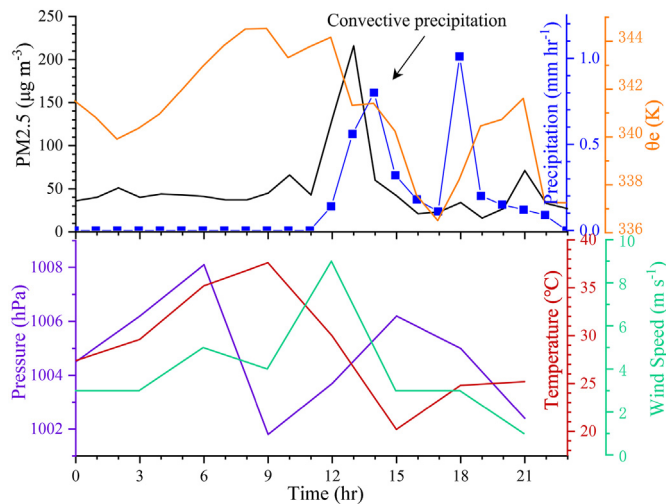
Fig. 2. Hourly evolution of $PM_{2.5}$ concentration ($\mu g\ m^{-3}$), GPM precipitation rate (mm/h), ERA5 near surface equivalent potential temperature (θ_e, K), air temperature (°C) at 2 m, wind speed (m s^{-1}) at 10 m and sea-level pressure (hPa) in Delhi on May 2.

the value at 11 UTC. Rainfall rises have matched the growth of $PM_{2.5}$ concentration with a lag of 1 h. Considering that surface equivalent potential temperature (θ_e) is conserved in the condensation and evaporation of water, numerous previous studies frequently used it to track convection (Betts et al., 2002; Wang et al., 2016). Here, the sharp decline in θ_e around the onset of precipitation suggested that the free tropospheric drier air was transported downward (i.e. convection occurred) at this time. Generally, the DCC and dust storm occurred almost at the same time and area, which is a terrific case to investigate the interplay between DCC and dust aerosol, so we call it "dust-rain storm". This study mainly focuses on the dust transport and development of deep convection in this area (black box in Fig. 1, 73–79°E, 27–35°N, here referred to study region).

3.2. Synoptic conditions for the development of dust-rain storm

This dust-rain storm is closely associated with the deep trough at 500 hPa over Kazakhstan. Cold air was taken from Arctic region to Central Asia by the strong northwesterly wind behind the trough and then gathered at this region. A shortwave trough, which is separated from the deep trough, protruded to Afghanistan at 00 UTC, resulting in a large temperature gradient at 850 hPa. At around noon time (06 UTC), with the southward extension and deepening of the shortwave trough, sea-level high pressure increased from 1025 hPa to 1030 hPa at Aral Sea, consistent with the closed high center at 850 hPa. The Pakistan and West India currently lied in front of the trough due to the eastward shift of deep trough at 500 hPa, which means the vertical motion is predominant. This weather pattern strengthened continuously at 12 UTC because of the strong sensible heating induced by solar radiation. The low pressure at surface even reduced to 997.5 hPa and air temperature reached more than 30 °C at 850 hPa over Pakistan and West India. Kumar et al. (2012) suggested that the dust storms happened easily under hotter and drier weather. Therefore, strong solar heating and cold front provoked the dust storms, leading to high dust emission over Thar desert on May 2.

Heavy precipitation is normally associated with proper dynamic conditions and adequate vapor supply. It is noteworthy that except for the lower to middle atmospheric circulation, the upper-level westerly jet shifted eastward from 77 °E at 00 UTC to 79 °E at 06 UTC. The upper-level westerly jet will induce a secondary circulation at exit zone of the jet stream, which pumps the air from surface to upper troposphere and provides vertical dynamics for the development of

thunderstorm. From the sounding in Delhi (Fig. S2a), there was a weak inversion layer below 850 hPa and the Convective Available Potential Energy (CAPE) was as high as 2538 J at morning (00 UTC). The cold advection started appearing below 700 hPa given that wind rotates counterclockwise with height. After the noon time (Fig. S2b), the air temperature near surface increased significantly to 40 °C and the air layer below 850 hPa reached superadiabatic state which means atmosphere stratification was pretty unstable. The higher temperature at 850 hPa even dominated the Thar desert and northwest India (Fig. 3). The humidity is also decreased with height between 850 hPa and 700 hPa. Such vertical thermal and moisture profile, the injection of dry and cold air at mid-troposphere, added the uplift of secondary circulation and cold front over study region, increased the CAPE to 3474 J and then triggered the convective cloud. According to the hourly evolution of ERA5 Skew-T-log plots, we found that near-surface temperature showed a downward trend due to surface cooling at night and the precipitation also occurred from 12 to 15 UTC (Fig. S3). Nevertheless, the CAPE rose to 3296 J at 16 UTC again, which further caused another precipitation process (Fig. 2). At the end of the day, the CAPE declines to minimum, representing the end of the rainfall.

In study region, easterly wind from the Bay of Bengal increased the moisture at low-level atmosphere (Fig. 4). The strong moisture input flux dominated the area and the value was over 10 g/(cm hPa s) before 7 UTC. Subsequently, it experienced a decline to half of the peak value at 9 UTC and almost terminated at 10 UTC. In contrast, the IWP of the total clouds increased to 3000 g m^{-2} continuously before 11 UTC, representing the development process of cloud top (Fig. 5). With considerable water supply, the thunderstorm occurred first at west of the study region before 6 UTC, and then moved to center at 7 UTC. It saw a remarkable enhancement from 8 to 9 UTC because the increment of IWP is higher in the study region despite the decrease in moisture transport. Heavy rainfall also occurred from 6 to 9 UTC with the rate of 2 mm/h and reached peak (over 5 mm/h) at 10 UTC, but decreased to 4 mm/h at 12 UTC (Fig. S4). Therefore, thunderstorm matured at 9 UTC and it did not weaken until 12 UTC. The thunderstorm began to move southeastward after 9 UTC and brought strong rainfall (Fig. S4).

Unlike the moisture which was taken by easterly wind from the Bay of Bengal, a large amount of dust aerosol from Thar desert was delivered towards study region continuously by prevailing southwesterly wind in front of low-level trough at 700 hPa (Fig. 4). The dust concentration also experienced a significant increase from 6 to 9 UTC, rising from 150 to 280 $\mu g\ m^{-3}$ and peaking at 12 UTC. Meanwhile, some dust aerosol moved out of study region to downstream, leading to thick dust layer as is shown in Fig. 1d. The dust transported to study region can be lifted to higher altitude by the vertical motion induced by cold front, upper-level westerly jet and surface convergence (Fig. 6). Undoubtedly, dust concentration over study region at 500 hPa is also pronounced with the peak value of over 60 $\mu g\ m^{-3}$ at 9 UTC, up from 45 $\mu g\ m^{-3}$, and persisted till 12 UTC (Fig. 5). Fig. 6 shows the vertical distribution of dust concentration and cloud ice water content from MERRA-2 and ERA5 reanalysis data, respectively. Dust from Thar desert aggregated at 700 hPa, resulting in a thick dust layer with dust concentration of over 220 $\mu g\ m^{-3}$ around 30°N. Supported by the converging ascending motion, a small portion of dust (around 60 $\mu g\ m^{-3}$) and massive moisture were lifted to 300 hPa and 200 hPa at 9 UTC, respectively, which is in favor of the interplay between dust and ice cloud. Although the dust concentration is weaker at 12 UTC due to the wet removal, this special vertical structure of dust and IWC is still obvious. Chen et al. (2020) elucidated that updraft in windward slope of Plateau is stronger compared with plain, and the southerly wind may intensify the updraft and bring more dust to the mountains, invigorating convective clouds via microphysical effect. Thus, it is possible for dust to participate in the formation of convective clouds by acting as IN or CCN over study region, which we will discuss below.
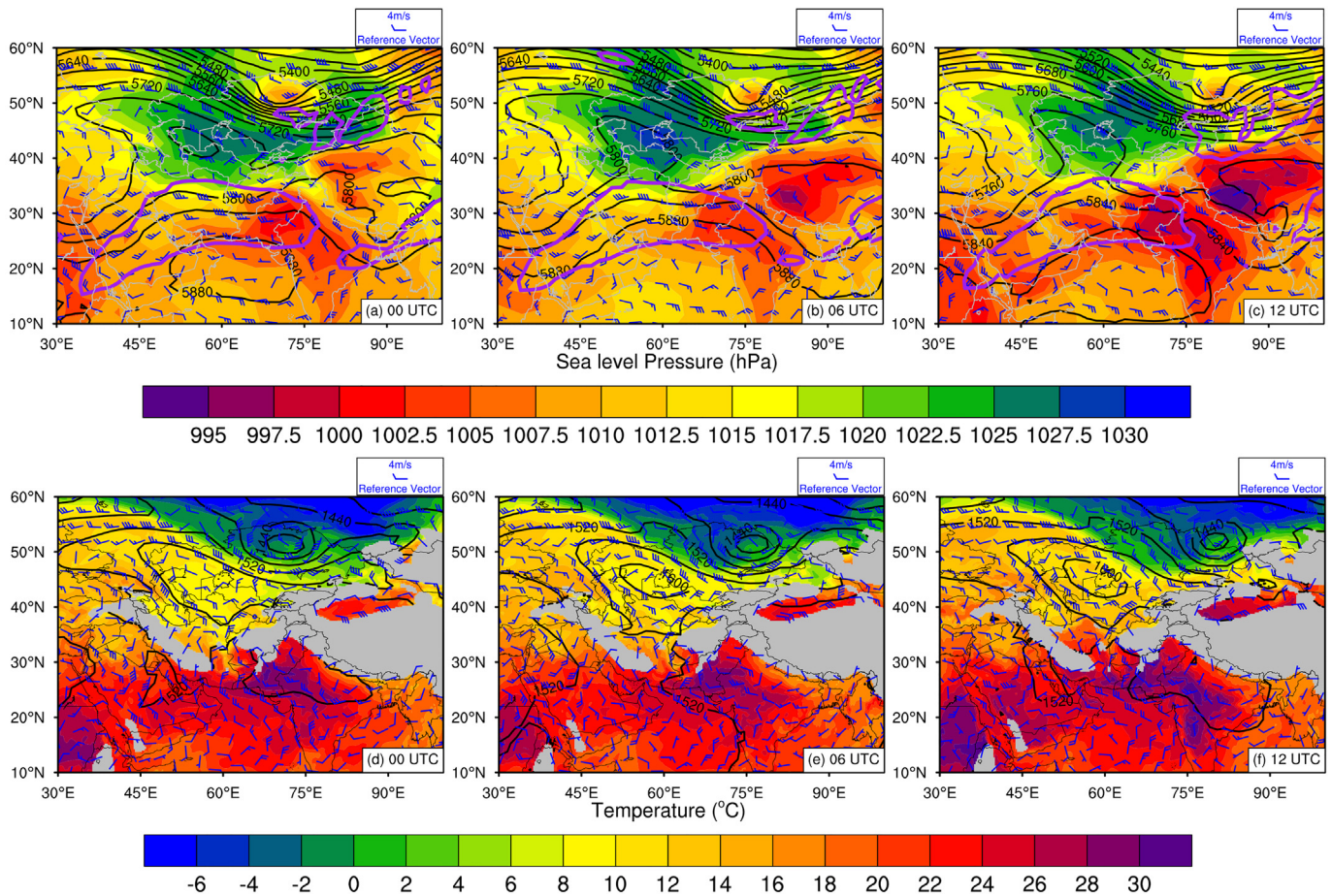
Fig. 3. Spatial distributions of geopotential height (black contour lines, gpm) and wind field (m s^{-1}) at 500 hPa, sea-level pressure (color scaled, hPa) and westerly jet at 200 hPa (zonal wind >30 m s^{-1}, purple contour lines) (top panel); and geopotential height (black contour lines, gpm), wind field (m s^{-1}) and air temperature (color scaled, °C) at 850 hPa (bottom panel) at 00, 06 and 12 UTC, May 2. Grey color indicates topography and the same applies to the following figures. (For interpretation of the references to color in this figure legend, the reader is referred to the web version of this article.)

3.3. Possible explanation for dust invigorating DCC by acting as IN

At the beginning of this section, we proposed a hypothesis on aerosol and deep convective cloud interaction. First of all, the DCC develops due to the strong water transport and appropriate atmospheric dynamics. When the convection is strong enough, more water vapor is transported above 0 °C isentropic layer rapidly. Soon, SWC formulates because of the shortage of CCN and IN. After dust particles are injected into this supercooled layer by convective updraft, some of them were activated as IN and transfer the SWC into ice cloud quickly. The cloud reflectance is expected to increase and cloud ice particle radius (IPR) intended to reduce when dust was lifted to upper levels of the clouds (Twomey effect, Twomey, 1977). Chakraborty et al. (2018) shed light on the critical role of latent heat release in the growth of deep convection from observations. As a result, the latent heat released by this freezing process is expected to strengthen the convection system, drawing more dust and vapor from surrounding region to the convective cloud. Consequently, the mature thunderstorm would cause heavy precipitation.

To put it in perspective, we tracked this process from CERES observations and MERRA-2 reanalysis data. Fig. 7 illustrates hourly evolution of cloud properties and dust AOD over study region on May 2. Dust AOD, COD and IWP showed an upward trend from 00 to 12 UTC with the figure rising to 0.4, 30 and 800 g m^{-2}, respectively. In particular, they experienced an abrupt rise between 6 and 9 UTC, which is consistent with the horizontal distribution in Section 3.2. Oppositely, the supercooled water path dropped from 254 g m^{-2} at 06 UTC to 17 g m^{-2} at 11 UTC. In spite of the high IPR (43.5 μm) at 4 UTC, it declined steeply to

27 μm at 9 UTC, implying the increase in ice cloud particle number. From this opposite time evolution, we can deduce that dust particles may be activated as effective IN, coagulating the supercooled water into ice cloud easily and quickly. This explanation can be again confirmed by the evolution of cloud particle phase which soared to 1.75, an increase of 0.25 over the period of 6 to 9 UTC. This change indicated that the liquid and mixed phase cloud was indeed transferred into ice cloud. The ability of dust aerosol to change cloud phase by providing effective IN was also found over northwestern East Asia where the frequency of dust storm is higher (Zhang et al., 2015; Yuan et al., 2019). The sufficient latent heating released from the freezing process plus the instability invigorated thunderstorm over study region and made more ice cloud appear at upper troposphere by strengthening the convection (Fig. 6b). As convective cloud matured, the heavy precipitation with the rate of over 5 mm/h began to occur after 9 UTC (Fig. S4). Similar phenomenon was also found by recent model simulation over north slopes of the Tibetan Plateau where dust particles caused the decrease in IPR, but increase in IWP, LWP and COD, hence intensifying the precipitation over northern area (Liu et al., 2020).

To gain more insight, Fig. 8 illustrates the reflectance of cirrus, ice cloud effective radius, supercooled cloud water path and AOD observed by MODIS at 6:30 and 8:05 UTC which approximately matches the time period of 6 and 8 UTC in Fig. 7, respectively. As the AOD in southwest margin of thunderstorm increased between two time periods, the ice cloud reflectance increased significantly, but the corresponding ice particle radius (over 32° E) that used to exist in the region east of 75° E and north of 30°N at 6:30 UTC decreased to around 16 μm at 08:05 UTC. The
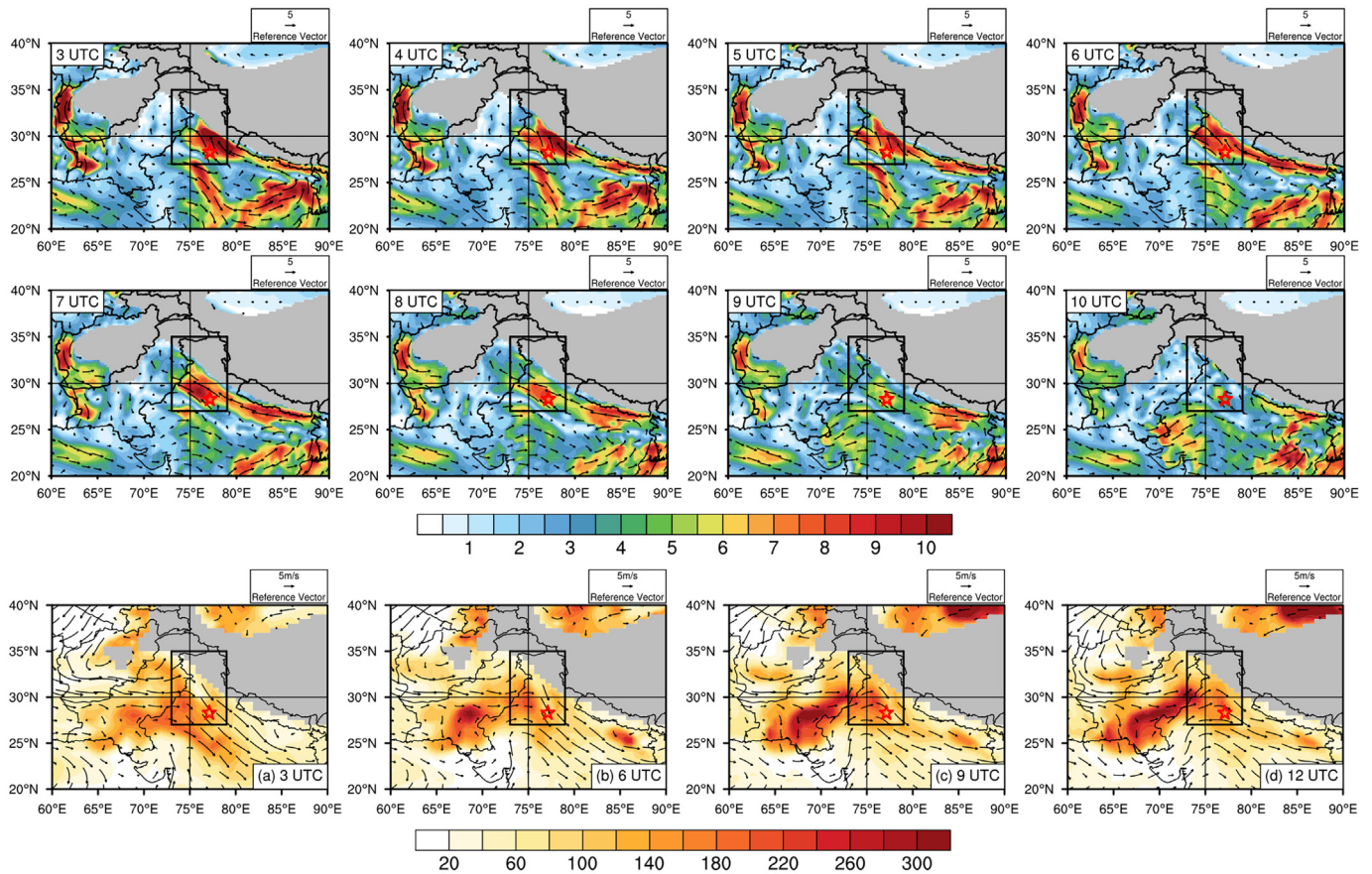
Fig. 4. Spatial distribution of EAR5 moisture flux (g cm^{-1} hPa^{-1} s^{-1}) at 850 hPa from 3 to 10 UTC, MERRA-2 dust concentration (μg m^{-3}) and wind vectors (m s^{-1}) at 700 hPa from 3 to 12 UTC, May 2.

supercooled cloud water path in the center also faded away as time went by. Identical conclusions were obtained in studies where Fromm et al. (2016) compared synoptic-scale baroclinic storm cloud property under dust-free conditions and impacted by long-range transport dust from eastern Asia and Sahara. They also suggested that CALIOP backscatter and attenuation of cirrus top was higher in dust-permeated cloud top compared with control counterparts. All of the evidences are in accord with the results derived from CERES data above.

Therefore, the engagement of dust aerosol IN may be partly responsible for the reduction of ice radius and increase in reflectance of cirrus in this DCC by changing cloud phase. Although the decline in ice cloud radius is coincident with our result, Huang et al. (2006) argued that dust aerosol from Taklimakan Desert resulted in the decrease of 32.8% and 42% in IWP and ice COD over arid or semi-arid region while the IWP and ice COD showed an upward trend in this study (Fig. 8 and Fig. S5). They speculated that the semi-direct effect or cloud evaporation contributed to this decline over the drier climate region, whereas in this study the contrary trends are possibly resulted from the sufficient moist from the Bay of Bengal and strong vertical motion. This is because cloud liquid water path increased with higher aerosol abundance over oceans where the moisture is rich (Albrecht, 1989; Khain et al., 2008; Qiu et al., 2017). Li et al. (2011) also summarized that aerosols contributed to precipitation in DCC when the liquid water content was higher, but suppressed it when the liquid water content was lower. Apart from moisture, it is also probably related to aerosol properties. By applying 9-year combined CloudSat radar and CALIPSO measurements, B. Zhao et al. (2018) found that dust and anthropogenic aerosols tend to increase COD of convection-generated ice clouds while it is false for smoke aerosols due to their strong solar absorbing capability which causes strong evaporation and suppresses convection.

4. Conclusion and discussion

This study analyzes a typical pre-monsoon dust-rain storm (a severe dust storm along with a thunderstorm) in Northwest India that erupted on May 2, 2018 by combining available satellite retrievals, in situ measurements and reanalysis data to investigate the effect of South Asian dust aerosol on DCCs. This special storm is the strongest over the past three decades regarding the adverse effect on human lives and properties and environment in northern India. The trough over Afghanistan and Pakistan divided from the deep trough over Kazakhstan brought cold air from North Pole to this region. Because of the strong solar heating around noon time, the coincidence of cold and warm air generated a cold front in Pakistan and northwest India. Therefore, dust storm occurred over Thar desert and moved northward towards study region where DCC rose almost at the same time with the joint effects of cold front, upper-level westerly jet, higher surface temperature and atmospheric instability. Dust aerosol was transported to study region by southwesterly wind at 700 hPa while moisture can be traced back to the Bay of Bengal via easterly wind at 850 hPa. Two branches converged over study region and then were lifted to mid-to-upper troposphere. Although CALIPSO tracks did not cross the center of thunderstorms, the mixing of dust and ice cloud, and SWC were retrieved over the south slops of Himalaya which adjoins study region before thunderstorms matured. Besides, OMI AAOD depicted that convective clouds were surrounded by thick dust layer. Thus, the dust signature near this thunderstorm implies enormous dust/hydrometeor mixing in the DCC.

Alam et al. (2014) investigated the correlation between AOD and cloud properties over Pakistan and suggested cloud top temperature and cloud top pressure correlated negatively with AOD in clod clouds but positively in warm clouds for all regions except Karachi. In Karachi,
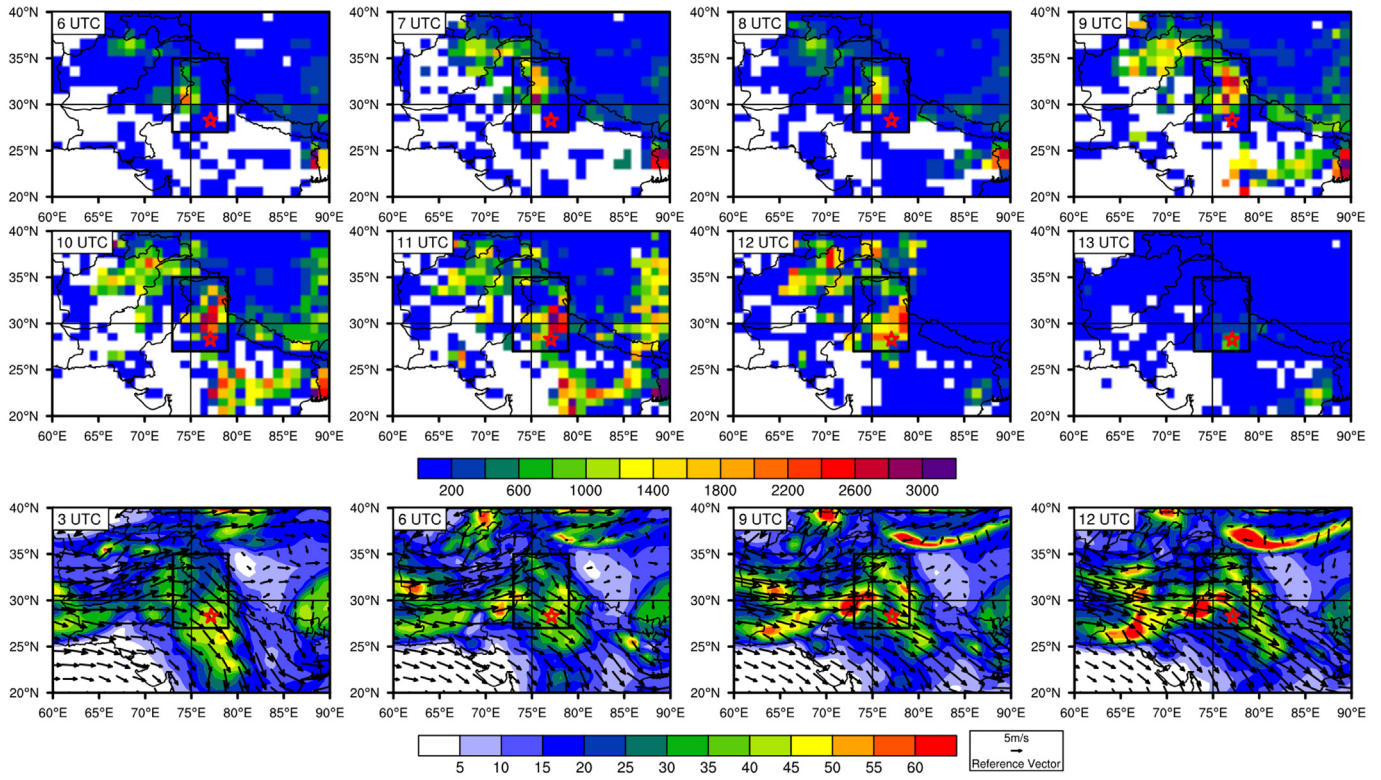
Fig. 5. Spatial distribution of total cloud IWP (g m^{-2}) derived from CERES from 3 to 10 UTC, MERRA-2 dust concentration (µg m^{-3}) and wind vectors (m s^{-1}) at 500 hPa from 3 to 12 UTC, May 2.
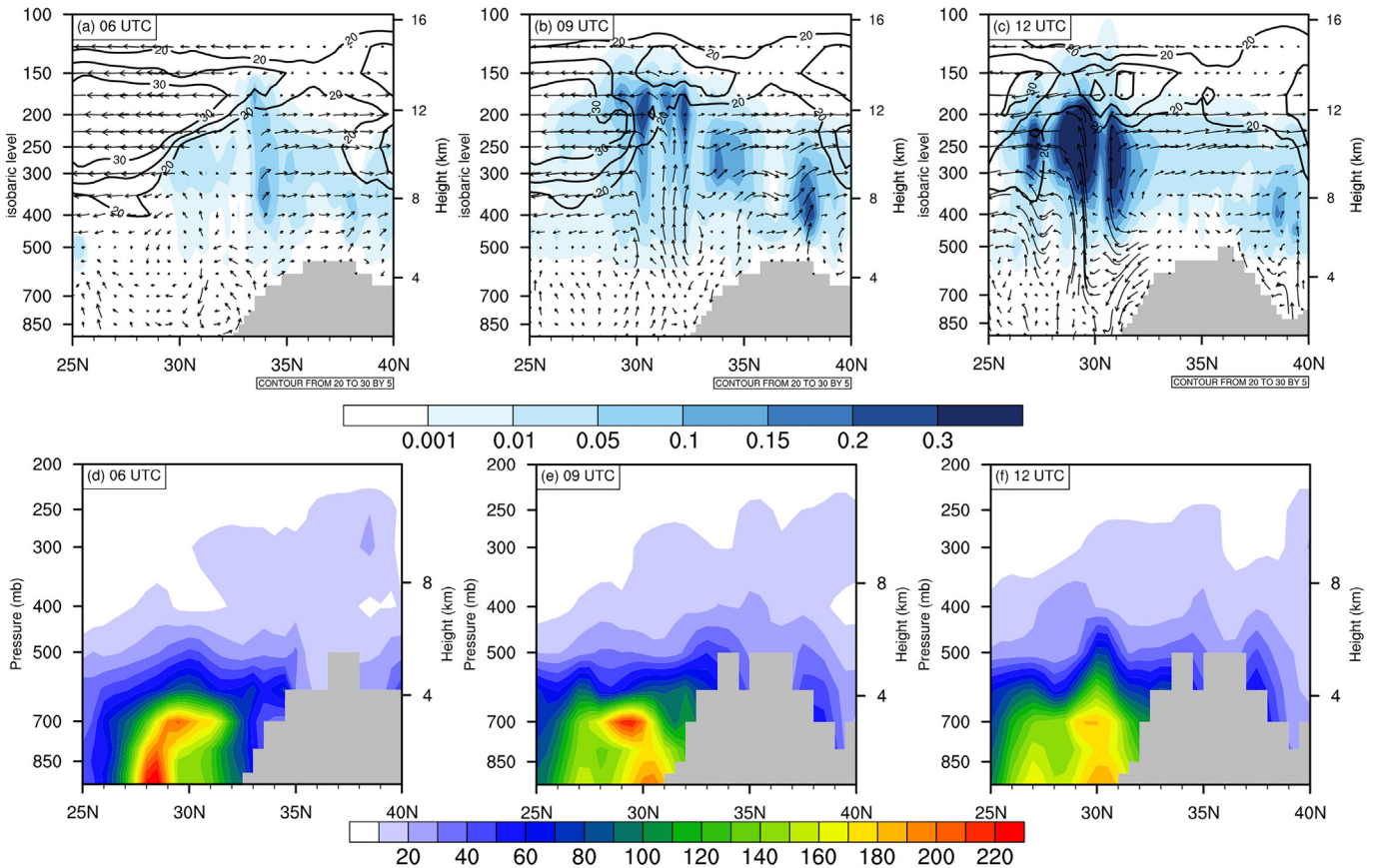
Fig. 6. Cross-section of cloud ice water content (color scaled, kg kg^{-1}), meridional circulation (vectors, m s^{-1}), zonal wind > 20 m s^{-1} (black contour lines, m s^{-1}) obtained from ERA5 reanalysis data (top panel) and MERRA-2 dust concentration (bottom panel, µg m^{-3}) along 75°E at 06, 09 UTC and 76.5°E at 12 UTC, respectively.
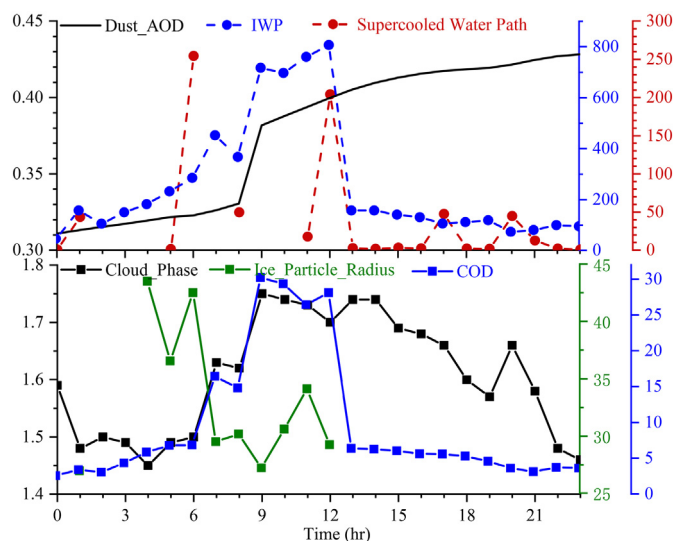
Fig. 7. Hourly evolution of MERRA-2 dust AOD, and cloud IWP (g m^{-2}), supercooled cloud water path (g m^{-2}), cloud phase, cloud ice particle radius (μm) and COD obtained from CERES averaged over study region on May 2.

the south region of Pakistan, dust aerosol and abundant moisture contributed to the high AOD in spring and summer (Alam et al., 2011). In the Himalaya Karakoram region, the highest AOD in spring months tended to increase COD and cloud fraction because of the sufficient humidity and high concentration of hydrophilic aerosols, but reduced cloud effective radius, resulting in suppression of precipitation process and surface cooling effect (Iftikhar et al., 2021). Based on the analysis of dust and microphysical cloud properties evolution, we concluded that South Asian dust may invigorate the convective clouds and enhance the rainfall through IN formation. This lies in the fact that the SWC reduced dramatically from 6 to 9 UTC when dust AOD, IWP and cloud phase demonstrated opposite trend, which suggests that dust particles are likely to be serving as IN and glaciate the liquid or mixed-phase clouds. Due to the injection of dust IN, the IPR derived from MODIS and CERES dropped considerably, sharing the similar characteristics with synoptic scale storm. The latent heat released from the phase-change process would further enhance the thunderstorm, thus, causing heavy rainfall by converging moisture. The increasing IN during dust storm was also used to demystify the cloud seeding experiments which enhanced the precipitation in different parts of convective clouds in Israel (Levi and Rosenfeld, 1996; Rosenfeld and Nirel, 1996). However, the cloud seeding effect on rainfall remains inconclusive and it is more difficult to identify the relationships between rainfall and aerosols compared with aerosol-cloud interaction (Levin and Cotton, 2007; Tao et al., 2012).

The invigoration of DCC by aerosols were also detected by TRMM over both land and continent and in the tropics, subtropics and mid-latitudes (Koren et al., 2012). Using TRMM rainfall data and AOD data during a tropical cyclone over western North Pacific, C. Zhao et al. (2018) demonstrated the increase in tropical cyclone rainfall rate and area as AOD increases. Aerosol invigoration effect is likely responsible for this observed evidence and then inclined to weaken tropical cyclone intensity by redistributing the latent heating (Zhang et al., 2009; Rosenfeld et al., 2012; Y. Wang et al., 2014). Wall et al. (2014) analyzed vertical structure of DCC systems in different land areas and found that the radar precipitation features from TRMM possessed taller echo tops, higher reflectivity, and lighten flashes under dirty background conditions in the Africa and Amazon regions compared to pristine conditions, whereas it shows different intensity for other regions. Using the same data, Chen et al. (2016) argued that radar reflectivity in shallow cloud was inhibited, while it was strengthened in the upper layer of deep

cumulus and DCC under polluted regimes in eastern China. The invigoration effect by aerosols is appearing in deep convective system regardless of thermodynamical conditions. Similarly, Guo et al. (2016) examined the internal structure of convective clouds over the Pearl River Delta of China and revealed that the convective precipitating clouds moved upward due to the increase in aerosol loading. Specifically, the top height of localized convective rain echo with 30 dBZ rose by ~1.27 km and the top radar reflectivity for convective rain regimes continues to increase, but reduces by ~0.47 km for the stratiform regime, as atmospheric pollution became serious (Guo et al., 2018). However, the physical mechanism behind this invigoration effect is still vague and our results may be one of the possible explanations. Guo et al. (2018) and Fan et al. (2009) inferred that wind shear might contribute to the invigoration effect, but the effect of meteorology on clouds cannot be totally eliminated (Chen et al., 2016).

Convective cloud properties show distinct responses to aerosol types (B. Zhao et al., 2018). Regarding dust aerosol, Min et al. (2009) gained an insight into its microphysical effect on the vertical structure of a deep convective precipitating cloud over the eastern Atlantic Ocean. Their results showed that some dust INs were transported to upper levels of cloud by robust convective updraft and enhanced convective precipitation, whereas other INs were transported to neighboring stratiform region by outflow, competing for available moisture. Consequently, the heavy precipitation was shifted to light precipitation, which is a little different from Guo et al. (2018). This is because the stratiform and convective regions in Min et al. (2009) appeared at a same DCC system and the final precipitation efficiency is the overall result of microphysical effects of dust aerosols in both regions (Li and Min, 2010). One of the key factors in this study that is different from Rosenfeld et al.'s (2008) model, is that the supercooled water is supposed to form due to the lack of CCN or intense convection at initial stage so that the dust aerosol can be lifted to upper level of cloud by strong convective updraft and activated as IN directly, which is similar to the process in convective region in Min et al. (2009). Otherwise, dust CCN may dominate this process. Rosenfeld et al. (2011) further highlighted that the phase-change of deep convective cloud initialed by dust IN would produce ice rainfall, counteracting the inhabitation of precipitation by CCN activity.

The effect of heterogeneous dust IN on cirrus can further alter the radiative budget with the radiative forcing of −0.24 to −1.59 W m^{-2} at the top of atmosphere estimated from Community Atmosphere Model CAM5 (M. Wang et al., 2014), and cause heavy precipitation in downstream (Zhao et al., 2020), which may be the reason why there was also heavy rainfall in Uttar Pradesh and other downwind regions during this event at night (Fig. S1). Although the possible effect of dust on deep convective cloud by serving as IN was explored in this study, we still cannot rule out the role of large-scale dynamics and vapor supply entrainment that determine the development of DCC and influence the multiple microphysical processes of deep clouds (Zhuang et al., 2018; Zhou et al., 2020). We also acknowledge that the dust CCN may also participate this process, but its contribution may be not as large as dust IN, given the robust change of cloud phase along with the increase in dust aerosol. Additionally, the uncertainties from data may also influence our conclusion. Although the bias between MERRA-2 and observation is reduced by assimilating the observed AOD, the AOD assimilation cannot constrain aerosol species and their vertical structure, and only had a limited effect in narrowing systematic biases (Buchard et al., 2017). Li et al. (2009) proposed that the cloud screening is one of the key factors of discrepancies when MODIS retrieve aerosol and clouds, while the CALIPSO and CloudSat were highly recommended for their active sensors. CALIPSO daytime products is also not reliable due to the interference of sunlight in comparison with nighttime counterparts. Despite the reasonable accuracy of CERES cloud properties, some large discrepancies in certain parameters like liquid water path, cloud phase and cloud-top height change is expected to cause uncertainty in our results (Minnis et al., 2011). Above all, we only proposed possible aerosol
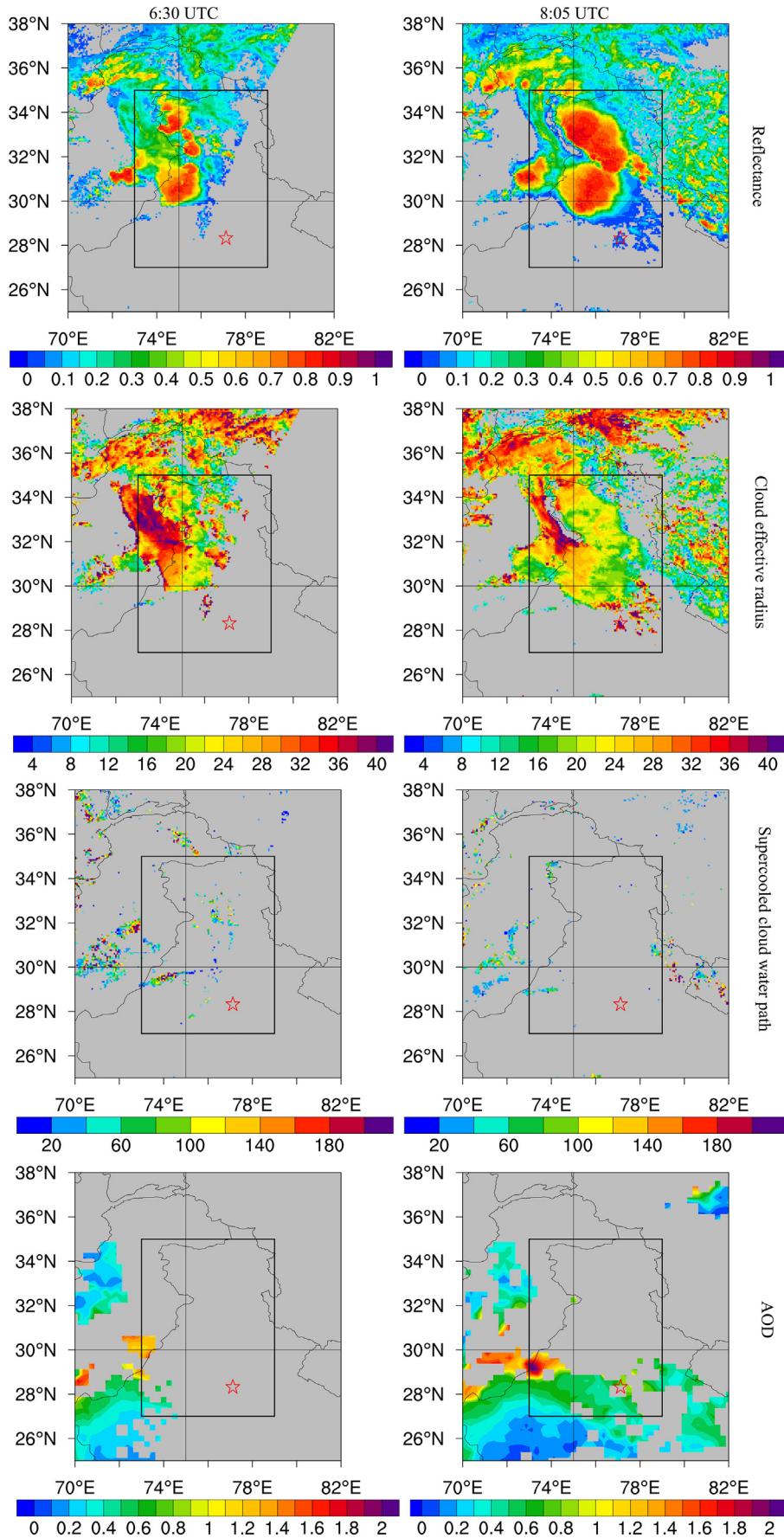
invigoration effect from observations, detailed mechanism for dust invigorating DCC as IN deserves to be better evaluated by model simulation, accurate and sufficient measurements in the future study.

CRediT authorship contribution statement

Tiangang Yuan: Conceptualization, Methodology, Formal analysis, Software, Validation, Writing – original draft, Writing – review & editing, Investigation. **Jianping Huang:** Methodology, Supervision, Writing – review & editing, Project administration. **Jiahui Cao:** Writing – original draft, Formal analysis, Software, Data curation. **Guolong Zhang:** Data curation. **Xiaojun Ma:** Data curation.

Declaration of competing interest

The authors declare that they have no known competing financial interests or personal relationships that could have appeared to influence the work reported in this paper.

Appendix A. Supplementary data

Supplementary data to this article can be found online at https://doi.org/10.1016/j.scitotenv.2021.146439.

References

Alam, K., Trautmann, T., Blaschke, T., 2011. Aerosol optical properties and radiative forcing over mega-city Karachi. Atmos. Res. 101 (3), 773–782. https://doi.org/10.1016/j.atmosres.2011.05.007.

Alam, K., Khan, R., Blaschke, T., Mukhtiar, A., 2014. Variability of aerosol optical depth and their impact on cloud properties in Pakistan. J. Atmos. Sol. Terr. Phys. 107, 104–112. https://doi.org/10.1016/j.jastp.2013.11.012.

Albergel, C., Dutra, E., Munier, S., Calvet, J.C., Munoz-Sabater, J., de Rosnay, P., Balsamo, G., 2018. ERA-5 and ERAInterim driven ISBA land surface model simulations: which one performs better? Hydrol. Earth Syst. Sci. 22, 3515–3532. https://doi.org/10.5194/hess-22-3515-2018.

Albrecht, B.A., 1989. Aerosols, cloud microphysics, and fractional cloudiness. Science 245, 1227–1230. https://doi.org/10.1126/science.245.4923.1227.

Betts, A.K., Gatti, L.V., Cordova, A.M., Dias, M., Fuentes, J.D., 2002. Transport of ozone to the surface by convective downdrafts at night. J. Geophys. Res. 107, 8046. https://doi.org/10.1029/2000JD000158.

Bodas-Salcedo, A., Hill, P.G., Furtado, K., Williams, K.D., Field, P.R., Manners, J.C., et al., 2016. Large contribution of supercooled liquid clouds to the solar radiation budget of the southern ocean. J. Clim. 29, 4213–4227. https://doi.org/10.1175/JCLI-D-15-0564.1.

Buchard, V., Randles, C.A., Da Silva, A.M., Darmenov, A., Colarco, P.R., Govindaraju, R., et al., 2017. The MERRA-2 aerosol reanalysis, 1980 onward. Part II: evaluation and case studies. J. Clim. 30, 6851–6872. https://doi.org/10.1175/jcli-d-16-0613.1.

Cesana, G., Chepfer, H., Winker, D., Getzewich, B., Cai, X., Jourdan, O., et al., 2016. Using in-situ airborne measurements to evaluate three cloud phase products derived from CALIPSO. J. Geophys. Res.-Atmos. 121 (10), 5788–5808. https://doi.org/10.1002/2015jd024334.

Chakraborty, S., Schiro, Kathleen A., Fu, R., David Neelin, J., 2018. On the role of aerosols, humidity, and vertical wind shear in the transition of shallow-to-deep convection at the Green Ocean Amazon 2014/5 site. Atmos. Chem. Phys. 18, 11135–11148. https://doi.org/10.5194/acp-18-11135-2018.

Chang, F.L., Minnis, P., Ayers, J.K., Mcgill, M.J., Palikonda, R., Spangenberg, D.A., et al., 2010. Evaluation of satellite-based upper troposphere cloud top height retrievals in multi-layer cloud conditions during TC4. J. Geophys. Res. 115, D00J05. https://doi.org/10.1029/2009JD013305.

Chen, S., Huang, J., Qian, Y., Zhao, C., Kang, L., Yang, B., Liu, Y., et al., 2017. An overview of mineral dust modeling over East Asia. J. Meteor. Res. 31, 633–653. https://doi.org/10.1007/s13351-017-6142-2.

Chen, T., Li, Z., Kahn, R.A., Zhao, C., Rosenfeld, D., Guo, J., et al., 2020. Potential impact of aerosols on convective clouds revealed by Himawari-8 observations over different terrain types in eastern China. Atmos. Chem. Phys. Discuss. https://doi.org/10.5194/acp-2020-845 [preprint]. (in review).

Chen, T.M., Guo, J.P., Li, Z.Q., Zhao, C., Liu, H., Cribb, M., et al., 2016. A CloudSat perspective on the cloud climatology and its association with aerosol perturbation in the vertical over East China. J. Atmos. Sci. 73, 3599–3616. https://doi.org/10.1175/JAS-D-15-0309.1.

DeMott, P.J., Sassen, K., Poellot, M.R., Baumgardner, D., Rogers, D.C., Brooks, S.D., et al., 2003. African dust aerosols as atmospheric ice nuclei. Geophys. Res. Lett. 30 (14), 1732. https://doi.org/10.1029/2003GL017410.

Dey, S., Tripathi, S.N., Singh, R.P., Holben, B.N., 2004. Influence of dust storms on the aerosol optical properties over the Indo-Gangetic basin. J. Geophys. Res. 109, D20211. https://doi.org/10.1029/2004JD004924.

Fan, J., Yuan, T., Comstock, J.M., Ghan, S., Khain, A., Leung, L.R., et al., 2009. Dominant role by vertical wind shear in regulating aerosol effects on deep convective clouds. J. Geophys. Res.-Atmos. 114, D22206. https://doi.org/10.1029/2009JD012352.

Fan, J., Rosenfeld, D., Zhang, Y., Giangrande, S.E., Li, Z., Machado, L.A., et al., 2018. Substantial convection and precipitation enhancements by ultrafine aerosol particles. Science 359, 411–418. https://doi.org/10.1126/science.aan8461.

Fang, J., Yang, W., Luan, Y., Du, J., Lin, A., Zhao, L., 2019. Evaluation of the TRMM 3B42 and GPM IMERG products for extreme precipitation analysis over China. Atmos. Res. 223, 24–38. https://doi.org/10.1016/j.atmosres.2019.03.001.

Fromm, M., Kablick III, G., Caffrey, P., 2016. Dust-infused baroclinic cyclone storm clouds: The evidence, meteorology, and some implications. Geophys. Res. Lett. 43, 12643–12650. https://doi.org/10.1002/2016GL071801.

Gautam, R., Liu, Z., Singh, R.P., Hsu, N.C., 2009. Two contrasting dust-dominant periods over India observed from MODIS and CALIPSO data. Geophys. Res. Lett. 36, L06813. https://doi.org/10.1029/2008GL036967.

Gautam, R., Hsu, N.C., Tsay, S.C., Lau, K.M., Holben, B., Bell, S., et al., 2011. Accumulation of aerosols over the indo-gangetic plains and southern slopes of the himalayas: distribution, properties and radiative effects during the 2009 pre-monsoon season. Atmos. Chem. Phys. 11, 12841–12863. https://doi.org/10.5194/acpd-11-15697-2011.

Gelaro, R., McCarty, W., Suárez, M.J., Todling, R., Molod, A., Takacs, L., Randles, C., et al., 2017. The modern-era retrospective analysis for research and applications. Version 2 (MERRA-2). J. Clim. 30 (14), 5419–5454. https://doi.org/10.1175/JCLI-D-16-0758.1.

Goswami, B.N., Venugopal, V., Sengupta, D., Madhusoodanan, M.S., Xavier, P.K., 2006. Increasing trend of extreme rain events over India in a warming environment. Science 314, 1442–1445. https://doi.org/10.1126/science.1132027.

Guo, J., Deng, M., Fan, J., Li, Z., Chen, Q., Zhai, P., et al., 2014. Precipitation and air pollution at mountain and plain stations in northern China: insights gained from observations and modeling. J. Geophys. Res.-Atmos. 119, 4793–4807. https://doi.org/10.1002/2013JD021161.

Guo, J., Deng, M., Lee, S.S., Wang, F., Li, Z., Zhai, P., et al., 2016. Delaying precipitation and lightning by air pollution over the Pearl River Delta. Part I: observational analyses. J. Geophys. Res.-Atmos. 121, 6472–6488. https://doi.org/10.1002/2015JD023257.

Guo, J., Liu, H., Li, Z., Rosenfeld, D., Jiang, M., Xu, W., Jiang, Jonathan H., et al., 2018. Aerosol-induced changes in the vertical structure of precipitation: a perspective of TRMM precipitation radar. Atmos. Chem. Phys. 18, 13329–13343. https://doi.org/10.5194/acp-18-13329-2018xx.

Heiblum, R.H., Koren, I., Altaratz, O., 2012. New evidence of cloud invigoration from TRMM measurements of rain center of gravity. Geophys. Res. Lett. 39, L08803. https://doi.org/10.1029/2012GL051158.

Hsu, N., Jeong, M., Bettenhausen, C., Sayer, A., Hansell, R., Seftor, C., et al., 2013. Enhanced Deep Blue aerosol retrieval algorithm: the second generation. J. Geophys. Res. Atmos. 118, 9296–9315. https://doi.org/10.1002/jgrd.50712.

Hu, Y., Winker, D., Vaughan, M., Lin, B., Omar, A., Trepte, C., et al., 2009. CALIPSO/CALIOP cloud phase discrimination algorithm. J. Atmos. Ocean. Technol. 26 (11), 2293–2309. https://doi.org/10.1175/2009jtecha1280.1.

Huai, B., Wang, J., Sun, W., Wang, Y., Zhang, W., 2021. Evaluation of the near-surface climate of the recent global atmospheric reanalysis for Qilian Mountains, Qinghai-Tibet Plateau. Atmos. Res. 250, 105401. https://doi.org/10.1016/j.atmosres.2020.105401.

Huang, J., Minnis, P., Lin, B., Wang, T., Yi, Y., Hu, Y., et al., 2006. Possible influences of Asian dust aerosols on cloud properties and radiative forcing observed from MODIS and CERES. Geophys. Res. Lett. 33, L06824. https://doi.org/10.1029/2005GL024724.

Fig. 8. Spatial distribution of reflectance (first row) and effective radius (μm, second row) for ice cloud, supercooled cloud water path (g m^{-2}, third row) and AOD at 550 nm (bottom row) observed from MODIS onboard Terra at 06: 30 UTC (left) and onboard Aqua at 08:05 UTC (right) May 2, respectively. (For interpretation of the references to color in this figure legend, the reader is referred to the web version of this article.)

Huang, J., Wang, T., Wang, W., Li, Z., Yan, H., 2014. Climate effects of dust aerosols over East Asian arid and semiarid regions. J. Geophys. Res. Atmos. 119, 11398–11416. https://doi.org/10.1002/2014JD021796.

Huang, J., Ji, M., Xie, Y., Wang, S., He, Y., Ran, J., 2016a. Global semi-arid climate change over last 60 years. Clim. Dyn. 46 (3–4), 1131–1150. https://doi.org/10.1007/s00382-015-2636-8.

Huang, J., Yu, H., Guan, X., Wang, G., Guo, R., 2016b. Accelerated dryland expansion under climate change. Nat. Clim. Chang. 6 (2), 166–171. https://doi.org/10.1038/nclimate2837.

Huang, J., Yu, H., Dai, A., Wei, Y., Kang, L., 2017a. Potential threats over drylands behind 2 °C global warming target. Nat. Clim. Chang. 7, 417–422. https://doi.org/10.1038/nclimate3275.

Huang, J., Li, Y., Fu, C., et al., 2017b. Dryland climate change: recent progress and challenges. Rev. Geophys. 55, 719–778. https://doi.org/10.1002/2016RG000550.

Huffman, G.J., Stocker, E.F., Bolvin, D.T., Nelkin, E.J., Jackson, Tan, 2019. GPM IMERG Final Precipitation L3 Half Hourly 0.1° × 0.1° V06. Goddard Earth Sciences Data and Information Services Center (GES DISC), Greenbelt, MD https://doi.org/10.5067/GPM/IMERG/3B-HH/06 Accessed: 10 July 2020.

Iftikhar, M., Alam, K., Adil Syed, W., Ahamd, M., Zeb, B., Liu, Y., Gulistan, N., 2021. Contrasting changes in cloud optical properties and the influence of aerosols, meteorology and radiation feedback in the Himalaya Karakoram region. Atmos. Res. 248, 105210. https://doi.org/10.1016/j.atmosres.2020.105210.

Jiang, Q., Li, W., Fan, Z., He, X., Sun, W., Chen, S., et al., 2020. Evaluation of the ERA5 reanalysis pitation dataset over Chinese Mainland. J. Hydrol. 2020, 125660. https://doi.org/10.1016/j.jhydrol.2020.125660 (In press).

Kedia, S., Ramachandran, S., Holben, B.N., Tripathi, S.N., 2014. Quantification of aerosol type, and sources of aerosols over the Indo-Gangetic Plain. Atmos. Environ. 98, 607–619. https://doi.org/10.1016/j.atmosenv.2014.09.022.

Kedia, S., Kumar, R., Islam, S., Sathe, Y., Kaginalkar, A., 2018. Radiative impact of a heavy dust storm over India and surrounding oceanic regions. Atmos. Environ. 185, 109–120. https://doi.org/10.1016/j.atmosenv.2018.05.005.

Khain, A.P., BenMoshe, N., Pokrovsky, A., 2008. Factors determining the impact of aerosols on surface precipitation from clouds: an attempt at classification. J. Atmos. Sci. 65, 1721–1748. https://doi.org/10.1175/2007JAS2515.1.

Kok, J., Ridley, D., Zhou, Q., Miller, R., Zhao, C., Heald, C., et al., 2017. Smaller desert dust cooling effect estimated from analysis of dust size and abundance. Nat. Geosci. 10, 274–278. https://doi.org/10.1038/ngeo2912.

Koren, I., Altaratz, O., Remer, L.A., Feingold, G., Martins, J.V., Heiblum, R.H., 2012. Aerosol-induced intensification of rain from the tropics to the mid-latitudes. Nat. Geosci. 5, 118–122. https://doi.org/10.1038/ngeo1364.

Kumar, R., Naja, M., Pfister, G.G., Barth, M.C., Brasseur, G.P., 2012. Simulations over South Asia using the Weather Research and Forecasting model with Chemistry (WRF-Chem): set-up and meteorological evaluation. Geosci. Model Dev. 5, 321–343. https://doi.org/10.5194/gmd-5-321-2012.

Kumar, R., Barth, M.C., Pfister, G.G., Naja, M., Brasseur, G.P., 2014. WRF-Chem simulations of a typical pre-monsoon dust storm in northern India: influences on aerosol optical properties and radiation budget. Atmos. Chem. Phys. 14, 2431–2446. https://doi.org/10.5194/acp-14-2431-2014.

Lau, K.M., Kim, M.K., Kim, K.M., 2006. Asian summer monsoon anomalies induced by aerosol direct forcing: the role of the Tibetan Plateau. Clim. Dyn. 26 (7–8), 855–864. https://doi.org/10.1007/s00382-006-0114-z.

Levi, Y., Rosenfeld, D., 1996. Ice nuclei, rainwater chemical composition, and static cloud seeding effects in Israel. J. Appl. Meteorol. 35, 1494–1501.

Levin, Z., Cotton, W., 2007. Aerosol Pollution Impact on Precipitation: A Scientific Review. Report from the WMO/IUGG International Aerosol Precipitation Science Assessment Group (IAPSAG). World Meteorological Organization, Geneva, Switzerland.

Li, R., Min, Q.-L., 2010. Impacts of mineral dust on the vertical structure of precipitation. J. Geophys. Res. 115, D09203. https://doi.org/10.1029/2009JD011925.

Li, Z., Zhao, X., Kahn, R., Mishchenko, M., Remer, L., Lee, K.-H., et al., 2009. Uncertainties in satellite remote sensing of aerosols and impact on monitoring its long-term trend: a review and perspective. Ann. Geophys. 27, 2755–2770. https://doi.org/10.5194/angeo-27-2755-2009.

Li, Z., Niu, F., Fan, J., Liu, Y., Rosenfeld, D., Ding, Y., 2011. Long-term impacts of aerosols on the vertical development of clouds and precipitation. Nat. Geosci. 4, 888–894. https://doi.org/10.1038/ngeo1313.

Li, Z., et al., 2016. Aerosol and monsoon climate interactions over Asia. Rev. Geophys. 54, 866–929. https://doi.org/10.1002/2015RG000500.

Liu, J., Zheng, Y., Li, Z., Cribb, M., 2011. Analysis of cloud condensation nuclei properties at a polluted site in southeastern China during the AMF-China Campaign. J. Geophys. Res. 116, D00K35. https://doi.org/10.1029/2011JD016395.

Liu, L., Huang, X., Ding, A., Fu, C., 2016. Dust-induced radiative feedbacks in north China: a dust storm episode modeling study using WRF-Chem. Atmos. Environ. 129, 43–54. https://doi.org/10.1016/j.atmosenv.2016.01.019.

Liu, L., Guo, J., Gong, H., Li, Z., Chen, W., Wu, R., et al., 2019. Contrasting influence of Gobi and Taklimakan deserts on the dust aerosols in Western North America. Geophys. Res. Lett. 46, 9064–9071. https://doi.org/10.1029/2019GL083508.

Liu, Y., Hua, S., Jia, R., Huang, J., 2019. Effect of aerosols on the ice cloud properties over the Tibetan Plateau. J. Geophys. Res.-Atmos. 124, 9594–9608. https://doi.org/10.1029/2019JD030463.

Liu, Y., Zhu, Q., Hua, S., Alam, K., Dai, T., Cheng, Y., 2020. Tibetan Plateau driven impact of Taklimakan dust on northern rainfall. Atmos. Environ. 234, 117583. https://doi.org/10.1016/j.atmosenv.2020.117583.

Min, Q., Li, R., Lin, B., Joseph, E., Wang, S., Hu, Y., Morris, V., Chang, F., 2009. Evidence of mineral dust altering cloud microphysics and precipitation. Atmos. Chem. Phys. 9, 3223–3231. https://doi.org/10.5194/acp-9-3223-2009.

Minnis, P., Sun-Mack, S., Young, D.F., Heck, P.W., Garber, D.P., Chen, Y., et al., 2011. CERES Edition-2 cloud property retrievals using TRMM VIRS and Terra and Aqua MODIS data, part I: algorithms. IEEE. T. Geosci. Remote. 49 (11), 4374–4400. https://doi.org/10.1109/TGRS.2011.2144601.

Pattanaik, D.R., Rajeevan, M., 2010. Variability of extreme rainfall events over India during southwest monsoon season. Meteorol. Appl. 17, 88–104. https://doi.org/10.1002/met.164.

Peng, J., Li, Z., Zhang, H., Liu, J., Cribb, M., 2016. Systematic changes in cloud radiative forcing with aerosol loading for deep clouds in the tropics. J. Atmos. Sci. 73, 231–249. https://doi.org/10.1175/JAS-D-15-0080.1.

Platnick, S.M., King, M.D., Ackerman, S.A., Menzel, W.P., Frey, R.A., 2003. The MODIS cloud products: algorithms and examples from terra. IEEE. T. Geosci. Remote. 41 (2), 459–473. https://doi.org/10.1109/TGRS.2002.808301.

Qiu, Y., Zhao, C., Guo, J., Li, J., 2017. 8-Year ground-based observational analysis about the seasonal variation of the aerosol-cloud droplet effective radius relationship at SGP site. Atmos. Environ. 164139-146. https://doi.org/10.1016/j.atmosenv.2017.06.002.

Ray, K., Giri, R.K., Ray, S.S., Dimri, A.P., Rajeevan, M., 2021. An assessment of long-term changes in mortalities due to extreme weather events in India: a study of 50 years' data, 1970–2019. Weather Clim. Extr. 32, 100315. https://doi.org/10.1016/j.wace.2021.100315.

Ray, Kamaljit, Arora, K., Srivastav, A., 2019. Weather extremes and agriculture. Int. Arch. Photogram. Rem. Sens. Spatial Inf. Sci. XLII-3/W6, 493–497. https://doi.org/10.5194/isprs-archives-XLII-3-W6-493-2019.

Rosenfeld, D., Nirel, R., 1996. Seeding effectiveness—the interaction of desert dust and the southern margins of rain cloud systems in Israel. J. Appl. Meteorol. 35, 1502–1510. https://doi.org/10.1175/1520-0450(1996)0352.0.CO;2.

Rosenfeld, D., Lohmann, U., Raga, G.B., O'Dowd, C.D., Kulmala, M., et al., 2008. Flood or drought: how do aerosol affect precipitation? Science 321, 1309–1313. https://doi.org/10.1126/science.1160606.

Rosenfeld, D., Yu, X., Liu, G., Xu, X., Zhu, Y., Yue, Z., et al., 2011. Glaciation temperatures of convective clouds ingesting desert dust, air pollution and smoke from forest fires. Geophys. Res. Lett. 38, L21804. https://doi.org/10.1029/2011GL049423.

Rosenfeld, D., Woodley, W.L., Khain, A., Cotton, W.R., Carrió, G., Ginis, I., Golden, J.H., 2012. Aerosol effects on microstructure and intensity of tropical cyclones. Bull. Am. Meteorol. Soc. 93 (7), 987–1001. https://doi.org/10.1175/BAMS-D-11-00147.1.

Roxy, M.K., Ghosh, S., Pathak, A., Athulya, A., Mujumdar, M., Murtugudde, R., et al., 2017. A threefold rise in widespread extreme rain events over central India. Nat. Commun. 8, 708. https://doi.org/10.1038/per.s41467-017-00744-9.

Sarkar, S., Chauhan, A., Kumar, R., Singh, R.P., 2019. Impact of deadly dust storms (May 2018) on air quality, meteorological, and atmospheric parameters over the northern parts of India. GeoHealth 3. https://doi.org/10.1029/2018GH000170.

Sijikumar, S., Aneesh, S., Rajeev, K., 2016. Multi-year model simulations of mineral dust distribution and transport over the Indian subcontinent during summer monsoon seasons. Meteorog. Atmos. Phys. 128, 453–464. https://doi.org/10.1007/s00703-015-0422-0.

Sikka, D.R., 1997. Desert climate and its dynamics. Curr. Sci. 72, 35–46.

Sun, E., Xu, X., Che, H., Tang, Z., Gui, K., An, L., et al., 2019. Variation in MERRA-2 aerosol optical depth and absorption aerosol optical depth over China from 1980 to 2017. J. Atmos. Sol. Terr. Phys. 186, 8–19. https://doi.org/10.1016/j.jastp.2019.01.019.

Sun, Y., Zhao, C., 2020. Influence of Saharan dust on the large-scale meteorological environment for development of tropical cyclone over North Atlantic Ocean Basin. J. Geophys. Res.-Atmos. 125, e2020JD033454. https://doi.org/10.1029/2020JD033454.

Tao, W.K., Chen, J.P., Li, Z.Q., Wang, C., Zhang, C.D., 2012. Impact of aerosols on convective clouds and precipitation. Rev. Geophys. 50, RG2001. https://doi.org/10.1029/2011RG000369.

Tobo, Y., Zhang, D., Matsuki, A., Iwasaka, Y., 2010. Asian dust particles converted into aqueous droplets under remote marine atmospheric conditions. Proc. Natl. Acad. Sci. U. S. A. 107, 17905–17910. https://doi.org/10.1073/pnas.1008235107.

Torres, O., 2008. OMI/Aura Near UV Aerosol Optical Depth and Single Scattering Albedo L3 1 day 1.0° × 1.0° V3. NASA Goddard Space Flight Center, Goddard Earth Sciences Data and Information Services Center (GES DISC) https://doi.org/10.5067/Aura/OMI/DATA3003 accessed 10 July 2020.

Twomey, S., 1977. The influence of pollution on the shortwave albedo of clouds. J. Atmos. Sci. 34, 1149–1152. https://doi.org/10.1175/1520-0469(1977)034<1149:TIOPOT>2.0.CO;2.

Wall, C., Zipser, E., Liu, C., 2014. An investigation of the aerosol indirect effect on convective intensity using satellite observations. J. Atmos. Sci. 71, 430–447. https://doi.org/10.1175/JAS-D-13-0158.1.

Wang, J., Krejci, R., Giangrande, S., Kuang, C., Barbosa, Henrique M.J., Brito, J., et al., 2016. Amazon Boundary Layer Aerosol Concentration Sustained by Vertical Transport during Rainfall. N. P. Web, United States https://doi.org/10.1038/nature19819.

Wang, Y., Lee, K.-H., Lin, Y., Levy, M., Zhang, R., 2014. Distinct effects of anthropogenic aerosols on tropical cyclones. Nat. Clim. Chang. 4 (5), 368–373. https://doi.org/10.1038/nclimate2144.

Wang, M., Liu, X., Zhang, K., Comstock, J.M., 2014. Aerosol effects on cirrus through ice nucleation in the Community Atmosphere Model CAM5 with a statistical cirrus scheme. J. Adv. Model. Earth Syst. 6, 756–776. https://doi.org/10.1002/2014MS000339.

Wang, T., Tang, J., Sun, M., Liu, X., Huang, Y., Huang, J., et al., 2020. Identifying a transport mechanism of dust aerosols over South Asia to the Tibetan Plateau: a case study. Sci. Total Environ. 758, 143714. https://doi.org/10.1016/j.scitotenv.2020.143714.

Wang, Z., Letu, H., Shang, H., Zhao, C., Li, J., Ma, R., 2019. A supercooled water cloud detection algorithm using Himawari-8 satellite measurements. J. Geophys. Res.-Atmos. 124, 2724–2738. https://doi.org/10.1029/2018JD029784.

Washington, R., Todd, M., Middleton, N.J., Goudie, A.S., 2003. Dust-storm source areas determined by the total ozone monitoring spectrometer and surface observations. Ann. Assoc. Am. Geogr. 93, 297–313. https://doi.org/10.1111/1467-8306.9302003.

Wielicki, B.A., Barkstrom, B.R., Harrison, E.F., Lee, R.B., Smith, G.L., Cooper, J.E., 1996. Clouds and the Earth's Radiant Energy System (CERES): an earth observing system experiment. Bull. Am. Meteorol. Soc. 77 (5), 853–868. https://doi.org/10.1175/1520-0477 (1996)077<0853:CATERE>2.0.CO;2.

Wu, J., Fu, C., Han, Z., Tang, J., Xu, Y., Zhang, R., 2010. Simulation of the direct effects of dust aerosol on climate in East Asia. Particuology 8, 301–307. https://doi.org/10.1016/j. partic.2010.01.006.

Xie, X., Liu, X., Che, H., Xie, X., Wang, H., Li, J., Shi, Z., Liu, Y., 2018. Modeling East Asian dust and its radiative feedbacks in CAM4-BAM. J. Geophys. Res.-Atmos. 123, 1079–1096. https://doi.org/10.1002/2017JD027343.

Yang, P., Hong, G., Kattawar, G.W., Minnis, P., Hu, Y., 2008. Uncertainties associated with the surface texture of ice particles in satellite-based retrieval of cirrus clouds: part II —effect of particle surface roughness on retrieved cloud optical thickness and effective particle size. IEEE. T. Geosci. Remote 46 (7), 1948–1957. https://doi.org/ 10.1109/tgrs.2008.916472.

Yang, X., Zhao, C., Yang, Y., 2020. Long-term multi-source data analysis about the characteristics of aerosol optical properties and types over Australia. Atmos. Chem. Phys. Discuss. https://doi.org/10.5194/acp-2020-921 [preprint]. (in review).

Yang, Y., Russell, L., Lou, M., Liao, S., Guo, H., Liu, J., et al., 2017. Dust-wind interactions can intensify aerosol pollution over eastern China. Nat. Commun. 8, 15333. https://doi. org/10.1038/ncomms15333.

Yang, Y., Zhao, C., Dong, X., Fan, G., Zhou, Y., Wang, Y., et al., 2019. Toward understanding the process-level impacts of aerosols on microphysical properties of shallow cumulus cloud using aircraft observations. Atmos. Res. 221, 27–33. https://doi.org/10.1016/j. atmosres.2019.01.027.

Yao, B., Teng, S., Lai, R., Xu, X., Yin, Y., Shi, C., Liu, C., 2020. Can atmospheric reanalyses (CRA and ERA5) represent cloud spatiotemporal characteristics? Atmos. Res. 244, 105091. https://doi.org/10.1016/j.atmosres.2020.105091.

Yao, W., Che, H., Gui, K., Wang, T., Zhang, X., 2020. Can MERRA-2 reanalysis data reproduce the three- dimensional evolution characteristics of a typical dust process in

East Asia? A case study of the dust event in May 2017. Remote Sens. 12, 902. https://doi.org/10.3390/rs12060902.

Yin, Y., Chen, L., 2007. The effects of heating by transported dust layers on cloud and precipitation: a numerical study. Atmos. Chem. Phys. 7, 3497–3505. https://doi.org/ 10.5194/acp-7-3497-2007.

Yuan, T., Chen, S., Huang, J., Wu, D., Lu, H., Zhang, G., et al., 2019. Influence of dynamic and thermal forcing on the meridional transport of Taklimakan Desert dust in spring and summer. J. Clim. 32 (3), 749–767. https://doi.org/10.1175/JcliD-18-0361.1.

Zhang, D., Liu, D., Luo, T., Wang, Z., Yin, Y., 2015. Aerosol impacts on cloud thermodynamic phase change over East Asia observed with CALIPSO and CloudSat measurements. J. Geophys. Res.-Atmos. 120, 1490–1501. https://doi.org/10.1002/2014JD022630.

Zhang, H., McFarquhar, G.M., Cotton, W.R., Deng, Y., 2009. Direct and indirect impacts of Saharan dust acting as cloud condensation nuclei on tropical cyclone eyewall development. Geophys. Res. Lett. 36, L06802. https://doi.org/10.1029/2009GL037276.

Zhao, B., Gu, Y., Liou, K.-N., Wang, Y., Liu, X., Huang, L., et al., 2018. Type-dependent responses of ice cloud properties to aerosols from satellite retrievals. Geophys. Res. Lett. 45, 3297–3306. https://doi.org/10.1002/2018GL077261.

Zhao, C., Lin, Y., Wu, F., Wang, Y., Li, Z., Rosenfeld, D., Wang, Y., 2018. Enlarging rainfall area of tropical cyclones by atmospheric aerosols. Geophys. Res. Lett. 45. https:// doi.org/10.1029/2018GL079427.

Zhao, C., Yang, Y., Fan, H., Huang, J., Fu, Y., Zhang, X., et al., 2020. Aerosol characteristics and impacts on weather and climate over the Tibetan Plateau. Natl. Sci. Rev. 7, 492–495. https://doi.org/10.1093/nsr/nwz184.

Zhou, S., Yang, J., Wang, W., Zhao, C., Gong, D., Shi, P., 2020. An observational study of the effects of aerosols on diurnal variation of heavy rainfall and associated clouds over Beijing–Tianjin–Hebei. Atmos. Chem. Phys. 20, 5211–5229. https://doi.org/10.5194/ acp-20-5211-2020.

Zhuang, Y., Fu, R., Wang, H., 2018. How do environmental conditions influence vertical buoyancy structure and shallow-to-deep convection transition across different climate regimes? J. Atmos. Sci. 75, 1909–1932. https://doi.org/10.1175/JAS-D-17-0284.1.